MULTISCALE HYDROLOGIC REMOTE SENSING

Perspectives and Applications

Edited by
Ni-Bin Chang
Yang Hong

CRC Press
Taylor & Francis Group
Boca Raton London New York

CRC Press is an imprint of the
Taylor & Francis Group, an **informa** business

2 Advanced Ground-Penetrating Radar for Soil Moisture Retrieval

Julien Minet, Khan Zaib Jadoon, François Jonard, Mohammad Reza Mahmoudzadeh, Phuong Anh Tran, and Sébastien Lambot

CONTENTS

2.1 Introduction 9
2.2 Soil Moisture Sensing by Ground-Penetrating Radar 11
2.3 Full-Waveform Inversion of GPR Data 12
2.3.1 Modeling of the GPR System 13
2.3.2 Inversion of GPR Data 14
2.3.3 Petrophysical Relationships 15
2.4 Validation and Applications 16
2.4.1 Mapping of Soil Moisture in Agricultural Fields 16
2.4.2 Comparison with the Direct Ground-Wave Method 19
2.4.3 Comparison with Ground-Based Radiometry 20
2.4.4 Soil Moisture Profile Characterization 22
2.4.5 Time-Lapse GPR Monitoring 23
2.4.6 Temporal Stability of Soil Moisture Patterns 25
2.5 Conclusions 26
Acknowledgments 27
References 27

2.1 INTRODUCTION

Soil moisture plays an important role in many environmental, agricultural, hydrologic, and climatic processes. In hydrology, soil moisture governs the partitioning of rainfall into runoff and infiltration, and neglecting its variability largely impacts on the prediction of solute leaching, erosion, runoff, and evaporation. In agriculture and irrigation applications, soil moisture is a crucial factor controlling plant growth and germination, particularly when saline stress is encountered. Knowing spatio-temporal distribution of soil moisture and soil water storage capacity is therefore an important asset for the optimization of irrigation under a variable environment. Soil moisture also exerts a strong control on soil biogeochemistry, especially with respect

to the cycling of nitrogen and carbon from soil to the hydrosphere, biosphere, and atmosphere. In climatology and meteorology, the importance of the soil moisture in the water balance and land surface energy budget has been widely acknowledged, as it controls the evaporation and the sensible heat fluxes between soil and atmosphere. In digital soil mapping applications, transitory soil moisture measurements at the field scale may actually provide information about (nearly) time-invariant soil attributes as soil hydraulic properties, which are dependent on soil structure and texture. Facing environmental contamination and increasing scarcity of resources, knowing the spatial variability of soil properties at the field scale at a high resolution is considerably appealing for designing new agricultural practices, in the framework of precision agriculture.

As it is exposed to continuously changing atmospheric forcing, soil moisture is highly variable in space and time. Determining its temporal and spatial variability is therefore essential for many scientific issues and applications from the field to the global scale. In that respect, a large number of soil moisture sensing techniques were used and developed in the last 50 years (Robinson et al. 2008a,b; Vereecken et al. 2008). The only direct soil moisture measurement method is the gravimetric method, which consists of weighing a soil sample before and after oven-drying it at 105°C. In the field of hydrogeophysics, numerous indirect methods for soil moisture sensing exist and rely on the measurement of a physical variable that is a surrogate for soil moisture. Most of these methods are based on the measurement of the soil response when it is exposed to electric current or electromagnetic field, depending on the soil electromagnetic properties. Two main categories of soil moisture measurement techniques are often distinguished: contact-based (or invasive) and contact-free methods (Vereecken et al. 2008). The contact-based methods require direct contact with the soil medium and include time-domain reflectometry (TDR) methods (Topp et al. 1980; Robinson et al. 2003), capacitance sensors (e.g., Bogena et al. 2007), electrical resistivity tomography (e.g., Michot et al. 2003), neutron probes (e.g., Hupet and Vanclooster 2002), heat pulse sensors (Campbell et al. 1991), and fiber optic sensors (e.g., Garrido et al. 1999). Recently, wireless sensor networks using clusters of invasive sensors have been deployed, offering the potentiality of measuring soil moisture over a large extent with high temporal resolution (Bogena et al. 2010).

Among the contact-free methods, we may distinguish between spaceborne or airborne remote sensing and proximal (or ground-based) sensing methods. There has been a huge development in recent years in remote sensing instruments and platforms for soil moisture. Methods of remote sensing of soil moisture include passive (radiometer) and active (scatterometer and synthetic aperture radar) microwave methods that operate at various spatial and temporal resolutions (Wigneron et al. 2003; Wagner et al. 2007). However, remote sensing methods still suffer from several limitations. Measurement capabilities are limited over dense vegetation cover and by the scattering effect of surface soil roughness (Verhoest et al. 2008; Jonard et al. in press) because of the relatively high frequencies at which these sensors usually operate. An important drawback is the shallow penetration depth of the remote sensing instruments (1–5 cm), whereas a deeper characterization of soil moisture is desirable in many applications (Capehart and Carlson 1997; Vereecken et al. 2008). Finally, the large-support scale of remote sensing techniques hides the within-pixel

soil moisture variability, which is generally resulting in a poor agreement with small-support scale calibrating measurements (e.g., Ceballos et al. 2005). The difference in support scales between large-scale remote sensing methods and small-scale invasive sensors may indeed reach several orders of magnitude, therefore making these two methods hardly comparable.

Proximal soil moisture sensing methods that are groundbased but noninvasive may bridge the scale gap that remains in soil moisture sensing techniques, making possible the characterization of soil moisture at an intermediate scale between remote sensing and invasive sensors. Proximal soil moisture sensing includes ground penetrating radar (GPR), electromagnetic induction sensors (e.g., Martinez et al. 2010), and ground-based radiometers (e.g., Jonard et al. 2011). Among these options, the GPR method for the determination of soil moisture was the most used and applied.

2.2 SOIL MOISTURE SENSING BY GROUND-PENETRATING RADAR

GPR is based on the propagation of a radar electromagnetic wave (typically in the range of 10–2000 MHz) into the ground. Wave propagation is governed by soil electromagnetic properties, that is, the dielectric permittivity ε, the electrical conductivity σ, and the magnetic permeability μ. For nonmagnetic soils as prevalent in the environment, μ is equal to the free-space magnetic permeability μ_0 and does not impact on the electromagnetic wave propagation. As the dielectric permittivity of water ($\varepsilon_w \approx 80$) is much larger than the one of the soil particles ($\varepsilon_s \approx 5$) and air ($\varepsilon_a = 1$), GPR wave propagation velocity in the soil is principally determined by its water content. GPR can image the soil with a high spatial resolution and up to a depth of several meters, depending on the frequency range of the electromagnetic waves. A review about recent development of GPR can be found in the work of Slob et al. (2010). In the areas of vadose zone hydrology and water resources management, GPR has been used to identify soil stratigraphy (Davis and Annan 1989; Grandjean et al. 2006), to locate water tables (Doolittle et al. 2006), to trace wetting front movement (Saintenoy et al. 2008), to identify soil hydraulic parameters (Binley et al. 2002; Cassiani and Binley 2005; Kowalsky et al. 2005; Jadoon et al. 2008; Lambot et al. 2009), to assess soil salinity (al Hagrey and Müller 2000), and to monitor contaminants (Cassidy 2007).

For soil moisture sensing, an excellent review of GPR applications was given by Huisman et al. (2003), where several methodologies of soil moisture determination using GPR wave propagation velocity or surface reflection were distinguished:

1. Determination of the wave propagation time to a known reflecting interface using a single-offset surface GPR (Grote et al. 2003; Lunt et al. 2005; van Overmeeren et al. 1997; Weiler et al. 1998)
2. Detection of the velocity-dependent reflecting hyperbola of a buried object using a single-offset surface GPR along a transect (Windsor et al. 2005)
3. Determination of the wave propagation velocity using multioffset surface GPR measurements above a reflecting layer (i.e., common midpoint method, Jacob and Hermance 2004)

4. Determination of the surface ground-wave velocity using multioffset and single-offset surface GPR (Huisman et al. 2002; Galagedara et al. 2003, 2005a,b; Grote et al. 2003, 2010)
5. Determination of the two-dimensional (2-D) spatial distribution of water by transmission tomography using borehole GPR (Binley et al. 2001; Alumbaugh et al. 2002; Looms et al. 2008)
6. Determination of the surface reflection coefficient using off-ground, air-launched GPR (Chanzy et al. 1996; Serbin and Or 2003, 2005)

Although these techniques are well established, they still suffer from major limitations originating from the strongly simplifying assumptions on which they rely with respect to electromagnetic wave propagation phenomena. As a result, a bias is introduced in the estimates due to the adequacy of a limited GPR model, and moreover, only a part of the information contained in the radar data is used, generally the propagation time. In addition, these techniques are not appropriate in a real-time mapping context, as usually, several cumbersome measurements are needed at a given location. According to Huisman et al. (2003), the main limitation of GPR methods may be the use of uncertain petrophysical relationships relating soil dielectric permittivity, which is directly retrieved from the GPR data, to soil moisture.

Recently, some authors have proposed innovative soil moisture retrieval techniques using the same GPR sensors. In that respect, Benedetto (2010) used a Rayleigh scattering-based method for directly determining the soil moisture, without the need of calibrating the GPR system or the petrophysical relationship. Oden et al. (2008) determined soil surface electromagnetic properties from early-time GPR wavelet analysis. Lastly, van der Kruk (2006) and van der Kruk et al. (2007) developed an inversion method of dispersed waveforms trapped in a surface waveguide (i.e., when the soil is layered by freezing, thawing, or a wetting front) for retrieving its dielectric permittivity and thickness. Inversion of GPR data coupled with an accurate electromagnetic model for wave propagation in GPR systems, including GPR antenna modeling, may therefore increase the retrieval capabilities from GPR data.

2.3 FULL-WAVEFORM INVERSION OF GPR DATA

A full-waveform electromagnetic model for the particular case of zero-offset, off-ground GPR was developed by Lambot et al. (2004a), where a single GPR antenna plays simultaneously the role of an emitter an and a receiver and is situated at some distance above the soil. The model includes propagation effects within the antenna and antenna–soil interactions, while this is usually not accounted for using common GPR methods, and an exact solution of three-dimensional (3-D) Maxwell's equations for wave propagation in multilayered media is considered, instead of the commonly used one-dimensional approach. Ultrawideband frequency-dependent GPR waveforms propagated to the soil are generated using a vector network analyzer (VNA). The main advantage of the VNA technology over traditional GPR systems is that the measured quantities constitute international standards and are well defined physically with proper calibration of the system. Soil electrical properties

are retrieved using an inversion of the filtered GPR waveform. Phase and amplitude information of the large-frequency-bandwidth GPR signal is inherently used for model inversion, thereby maximizing information retrieval from the available radar data, both in terms of quantity and quality. The technique was validated in a series of hydrogeophysical applications (Lambot et al. 2004a,b, 2006, 2008, 2009; Jadoon et al. 2008, 2010; Minet et al. 2010, 2011; Jonard et al. 2011).

2.3.1 Modeling of the GPR System

The GPR signal to be modeled consists of the frequency-dependent complex ratio $S_{11}(\omega)$ between the returned signal and the emitted signal, with ω being the angular frequency. It relies on the linearity of Maxwell's equations and assumes that the spatial distribution of the backscattered electromagnetic field measured by the antenna does not depend on the subsurface, that is, only the amplitude and phase change. This is expected to be a valid assumption if the antenna is not too close to the ground, given that the soil can be described by a planar layered medium. The model consists of a linear system composed of elementary model components in series and parallel, all characterized by their own frequency response function accounting for specific electromagnetic phenomena. The resulting transfer function relating $S_{11}(\omega)$ measured by the VNA to the frequency response $G_{xx}^{\uparrow}(\omega)$ of the multilayered medium is expressed in the frequency domain by

$$S_{11}(\omega) = \frac{b(\omega)}{a(\omega)} = H_i(\omega) + \frac{H(\omega)G_{xx}^{\uparrow}(\omega)}{1 - H_f(\omega)G_{xx}^{\uparrow}(\omega)}, \tag{2.1}$$

where $b(\omega)$ and $a(\omega)$ are, respectively, the received and emitted signals at the VNA reference calibration plane; $H_i(\omega)$, $H(\omega)$, and $H_f(\omega)$ are, respectively, the complex return loss, transmitting–receiving, and feedback loss transfer functions of the antenna; and $G_{xx}^{\uparrow}(\omega)$ is the transfer function of the air–subsurface system modeled as a multilayered medium (referred to as Green's function below). Owing to inherent variations in the impedance between the antenna feed point, antenna aperture, and air, multiple wave reflections occur within the antenna. Under the assumption above, these reflections can be accounted for exactly using the antenna transfer functions, which thereby play the role of frequency-dependent, global reflection, and transmission coefficients. In that way, the proposed model inherently takes into account the multiple wave reflections occurring between the antenna and the soil. The antenna transfer functions are determined in the laboratory using measurements in known medium and antenna configuration. These antenna transfer functions inherently account for the frequency-dependent phase center (Jadoon et al. 2011). Using these antenna transfer functions, the measured Green's function $G_{xx}^{\uparrow}(\omega)$ that depends solely on the medium can be derived from the raw measured data $S_{11}(\omega)$ using

$$G_{xx}^{\uparrow}(\omega) = \frac{-S_{11}(\omega) + H_i(\omega)}{H_i(\omega)H_f(\omega) - S_{11}(\omega)H_f(\omega) - H(\omega)}. \tag{2.2}$$

The solution of Maxwell's equations for electromagnetic waves propagating in multilayered media is well known. Following the approach of Lambot et al. (2004a), the analytic expression for the zero-offset Green's function in the spectral domain (2-D spatial Fourier domain) is found to be

$$\tilde{G}_{xx}^{\uparrow} = \left(\frac{\Gamma_n R_n^{\mathrm{TM}}}{\eta_n} - \frac{\xi_n R_n^{\mathrm{TE}}}{\Gamma_n} \right) \exp(-2\Gamma_n h_n), \tag{2.3}$$

where the subscript n equals 1 and denotes the first interface and first layer (in practice, the air layer); R_n^{TM} and R_n^{TE} are, respectively, the transverse magnetic (TM) and transverse electric (TE) global reflection coefficients (Slob and Fokkema 2002) accounting for all reflections and multiples from surface and subsurface interfaces; Γ_n is the vertical wave number defined as $\Gamma_n = \sqrt{k_\rho^2 + \xi_n \eta_n}$; k_ρ is a spectral-domain transform parameter; $\xi_n = j\omega\mu_n$; $\eta_n = \sigma_n + j\omega\varepsilon_n$; and $j = \sqrt{-1}$.

The transformation of Equation 2.3 from the spectral domain to the spatial domain is carried out by employing the 2-D Fourier inverse transformation:

$$G_{xx}^{\uparrow} = \frac{1}{4\pi} \int_0^{+\infty} \tilde{G}_{xx}^{\uparrow} \, dk_\rho, \tag{2.4}$$

which reduces to a single integral in view of the invariance of the electromagnetic properties along the x- and y-coordinates. We developed a specific procedure to properly evaluate that singular integral using an optimal integration path (Lambot et al. 2007). In addition to avoiding the singularities (branch points and poles), the path allows for minimizing the oscillations of the complex exponential part of the integrand, which makes the integration faster.

2.3.2 Inversion of GPR Data

Inversion of Green's function is formulated by the complex least squares problem as follows:

$$\min \phi(\mathbf{b}) = \left| \mathbf{G}_{\mathbf{xx}}^{\uparrow *} - \mathbf{G}_{\mathbf{xx}}^{\uparrow} \right|^{T} \mathbf{C}^{-1} \left| \mathbf{G}_{\mathbf{xx}}^{\uparrow *} - \mathbf{G}_{\mathbf{xx}}^{\uparrow} \right|, \tag{2.5}$$

where $\mathbf{G}_{\mathbf{xx}}^{\uparrow *} = G_{xx}^{\uparrow}(\omega)$ and $\mathbf{G}_{\mathbf{xx}}^{\uparrow} = G_{xx}^{\uparrow}(\omega, \mathbf{b})$ are vectors containing, respectively, the observed and simulated radar measurements, from which major antenna effects have been filtered using Equation 2.1; $\mathbf{C}$ is the error covariance matrix; and $\mathbf{b}$ is the parameter vector containing the soil electromagnetic parameters, which are the soil relative dielectric permittivity ε and electrical conductivity, and layer thicknesses to be estimated. As function $\phi(\mathbf{b})$ has usually complex topography, we use the global multilevel coordinate search algorithm (Huyer and Neumaier 1999) combined

sequentially with the classical Nelder–Mead simplex algorithm (Lagarias et al. 1998) for minimizing the function.

2.3.3 Petrophysical Relationships

A petrophysical relationship is necessary for translating the optimized dielectric permittivity ε from GPR data inversion into volumetric soil moisture θ. Reviews of ε–θ relationships can be found in the works of Huisman et al. (2003), Robinson et al. (2003), Ponizovsky et al. (1999), Fernandez-Galvez (2008), and Steelman and Endres (2011). Generally, petrophysical relationships are developed by two main approaches. The first approach is empiric and uses measurements of dielectric permittivity for a variety of soil types at different water contents to construct the regressive polynomial formulas relating the water content to the dielectric permittivity. The most frequently used empirical formula is the relationship suggested by Topp et al. (1980):

$$\theta = -5.3\times10^{-2} + 2.92\times10^{-2}\varepsilon - 5.5\times10^{-4}\varepsilon^2 + 4.3\times10^{-6}\varepsilon^3. \tag{2.6}$$

This equation has been widely applied to predict soil moisture from TDR and GPR measurements, and its validity was established in many studies (Drungil et al. 1989; Hallikainen et al. 1985; Roth et al. 1992). However, its applicability appeared to be poor for organic, clayey, and fine-textured soils (Dirksen and Dasberg 1993; Todoroff and Langellier 1998; Ponizovsky et al. 1999).

The second approach is more theoretical and derives the water content from dielectric mixing models of soil. According to this approach, soil is a complex mixture of air, water, and soil particles. The permittivity of soil, therefore, is predicted from the permittivity of each component weighted by their volume fraction. A general formulation of a commonly adopted dielectric mixing model is the power law model:

$$\varepsilon = \left(\theta\varepsilon_w^\alpha + (\phi-\theta)\varepsilon_a^\alpha + (1-\phi)\varepsilon_s^\alpha\right)^{1/\alpha}, \tag{2.7}$$

in which ϕ is the soil porosity; ε_a, ε_w, and ε_s are the permittivities of air, water, and soil particles, respectively; and α is the empirical power coefficient of the equation, which holds for the spatial structure of soil mixture and its orientation with respect to the electromagnetic field. Different power coefficients were proposed based on calibration with empirical data. Birchak et al. (1974) used the coefficient of 0.5, which is widely known as the complex refractive index model (CRIM). CRIM was also confirmed by Shutko and Reutov (1982), Roth et al. (1990), and Gorriti (2004) as the most suitable power law model. By contrast, Dobson et al. (1985) found that $\alpha = 0.65$ enabled describing the complex permittivity at the frequency range from 1.4 to 18 GHz for different soil types. Compared to empirical formulas, this approach takes into account the composition of soil materials, and thus, it is expected to better predict the water content. However, in order to estimate the water content, the approach

requires prior knowledge of the porosity of the soil material and permittivities of the individual constituents.

2.4 VALIDATION AND APPLICATIONS

The developed GPR method was widely validated in laboratory experiments in different soil configurations, including two-layered soil structure (Lambot et al. 2004a), shallow soil layering (Lambot et al. 2006; Minet et al. 2010), continuously varying soil moisture profile (Lambot et al. 2004b), and the presence of high electrical conductivity (Lambot et al. 2006). Herein, validation and applications of the GPR method for soil moisture sensing and mapping in field conditions are presented.

2.4.1 Mapping of Soil Moisture in Agricultural Fields

An important asset of using off-ground GPR in proximal soil sensing applications is that no contact with soil is required, thereby allowing for fast acquisition without "stop-and-go" of the acquisition platform. For field acquisition, the GPR system was mounted on an all-terrain vehicle (ATV) with an accurate Global Positioning System (GPS). Figure 2.1 presents the ATV holding the GPR system, which is composed of the VNA and an ultrawideband horn antenna (frequency range of 200–2000 MHz), the GPS, and a PC integrating the measurements. Using this mobile platform, GPR measurements can be acquired at a high resolution (~1 m) over a large extent (several hectares) within a limited time frame (>1000 measured points/h). GPR inversion allows for retrieving soil dielectric permittivity values that were translated in soil moisture using Equation 2.6 and then interpolated. Soil

FIGURE 2.1 ATV holding the GPR, the GPS, and a PC. The GPR horn antenna is situated at the back of the ATV at around 1 m above the soil surface.

moisture is measured within an antenna footprint of about 1 m^2 and with a penetration depth of about 10 cm.

Using the GPR mounted on the ATV, we acquired 3572 GPR point measurements in a 5.5-ha agricultural field in Cruchten, Luxembourg, on 13 March 2009. The soil was bare with little vegetation and limited surface roughness, as neither tillage nor other field work was performed for 5 months. Soil moisture was retrieved by an inversion (see Equation 2.5) of the filtered GPR data, with soil modeled as a homogeneous medium. In order to validate the soil moisture estimates, soil samples for gravimetric measurements were taken in 31 regularly spaced locations across the field. Figure 2.2 presents the surface soil moisture map from the interpolation of point measurements using ordinary kriging.

The soil moisture pattern appeared to be mainly explained by soil texture, as the driest areas in the northwest of the field were characterized by a larger sand fraction that may increase the soil hydraulic conductivity and gave rise to a faster drying in the surface. As the field was rather flat, no water redistribution seemed to occur, and the soil moisture pattern was not determined by topography. Figure 2.3 shows the comparison between interpolated GPR-derived dielectric permittivity and soil moisture measurements using gravimetric measurements. A Topp's-like petrophysical relationship (Equation 2.5) was fitted over the data. There was a very good agreement between these two variables, with a root mean square error (RMSE) of 0.023 m^3/m^3. The residual discrepancies were mainly attributed to the different support scales of the two soil moisture measurement techniques with respect to the small-scale spatial variability of soil moisture and to the different penetration depths.

In that respect, in another field experiment using the same GPR system, Jadoon et al. (2010) performed several GPR and TDR measurements along a transect, with five TDR measurements within each GPR footprint. Figure 2.4 presents the comparison

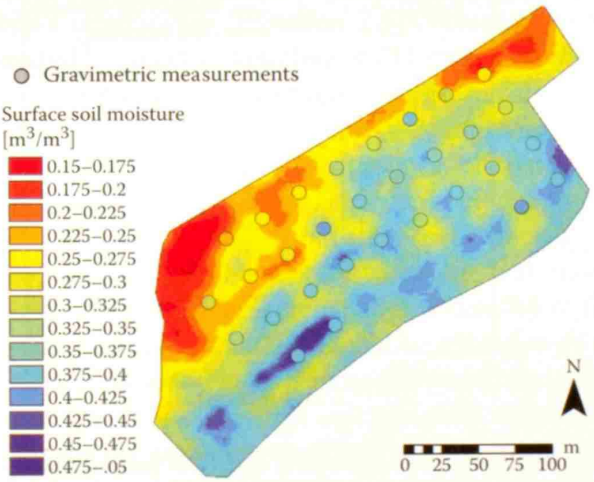

FIGURE 2.2 Soil moisture map from interpolated GPR soil moisture measurement in Cruchten, Luxembourg, 13 March 2009. Soil moisture values from gravimetric measurements are displayed on the map with the same color range.

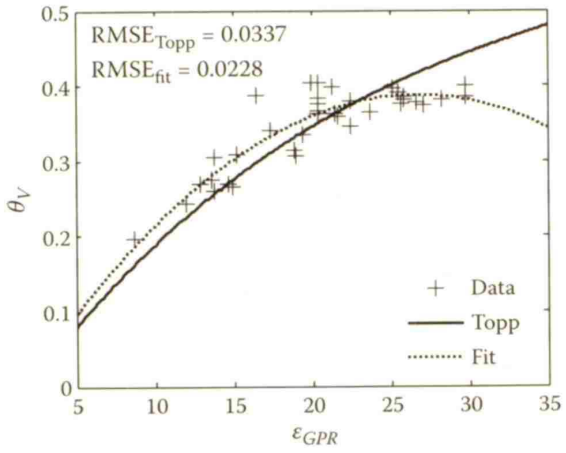

FIGURE 2.3 Comparison between interpolated GPR-derived dielectric permittivity and ground-truth soil moisture measurements for the field campaign in Cruchten.

between GPR and TDR estimates along the transect. A general decrease in soil moisture along the transect can be observed with both methods. While an RMSE between TDR and GPR estimates of only 0.025 m^3/m^3 was found, a soil moisture variability of 0.02–0.07 m^3/m^3 was measured by TDR within GPR footprints. Soil moisture measured by the GPR is therefore the integration of the small-scale soil moisture variability within the footprint.

In another field experiment, the repeatability of the GPR method for soil moisture sensing was evaluated by performing three repetitions of GPR measurements in a

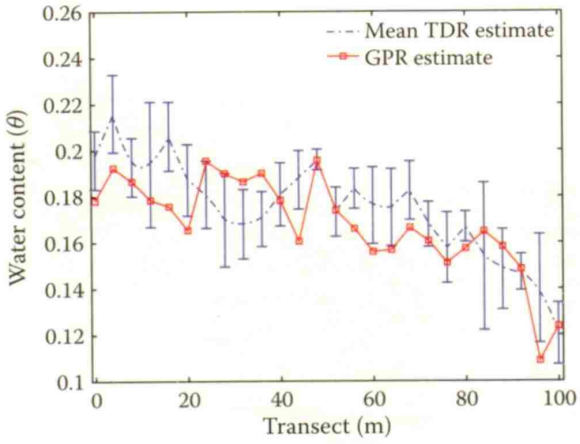

FIGURE 2.4 Soil moisture inferred from GPR and TDR measurements. The solid line and dashed–dotted line represent, respectively, the soil moisture inferred by GPR and mean soil moisture estimated from five TDR measurements. (Adapted from Jadoon, K. Z. et al., *Near Surface Geophysics*, 8(6), 483–491, 2010.)

2.5-ha field within 3 h. The repeatability error was equal to 0.017 m^3/m^3 and was mainly attributed to the interpolation uncertainties, as GPR measurements were not taken exactly at the same locations between the repetitions. The GPR method for soil moisture sensing appeared highly precise and reproducible owing to the accurate modeling of the GPR system and the high-quality information that is recorded by VNA over a large frequency bandwidth.

2.4.2 Comparison with the Direct Ground-Wave Method

The off-ground GPR method was compared with the commonly used ground-wave method using on-ground GPR (e.g., Galagedara et al. 2003) for soil moisture sensing in field conditions. In a bistatic GPR system (i.e., composed of transmitting and receiving antennas), the GPR ground wave is the signal traveling directly from a transmitting to a receiving antenna through the upper centimeters of the soil, and it is the only wave of which the propagation distance can be known *a priori*. GPR ground wave can thus be used for determining soil moisture without knowledge of soil depth or in the absence of any method that clearly reflects soil interface. Ground waves can be identified from single trace analysis (STA) acquisitions, where the transmitting and receiving antennas are separated by a fixed antenna separation (single-offset GPR). Compared to multioffset GPR methods, the STA approach is more appropriate for mapping large areas owing to its practicability (Lehmann and Green 1999).

A 5-ha field near Bastendorf, Luxembourg, was surveyed using the two GPR methods in September 2010, a few hours after a precipitation event. A pulse radar combined with a pair of 400-MHz bow-tie antennas was used for ground-wave acquisition. The dielectric permittivity was derived from the ground-wave velocity using the STA approach. For the off-ground GPR, the dielectric permittivity was retrieved using inversion of the radar data in the time domain, focusing on the surface reflection. Dielectric permittivities were then translated in volumetric soil moisture using Topp's relationship (Equation 2.5). Volumetric soil moisture was independently measured by soil core sampling at 27 locations across the field. Figure 2.5 compares the soil moisture maps derived from the off-ground GPR inversion and ground-wave on-ground GPR method. There was an overall good agreement in the average soil moisture between the two techniques, but particular soil moisture patterns appeared different. These discrepancies could be due to the different penetration depths of the two GPR methods. In that respect, the off-ground GPR may sense the first 5 cm, whereas the ground-wave technique may reflect soil moisture from larger depths (up to 20 cm). The larger spatial variability of the soil moisture, which is observed with the off-ground GPR, could be related to its shallow depth of characterization, as the shallow soil layer is more influenced by varying atmospheric conditions than the deeper layer. The high soil moisture values that are sensed at the east of the field by the off-ground method may also originate from the shallower characterization of the off-ground GPR, as the survey was following a precipitation event. The soil sampling locations and corresponding volumetric soil moisture values are depicted with circles on the maps.

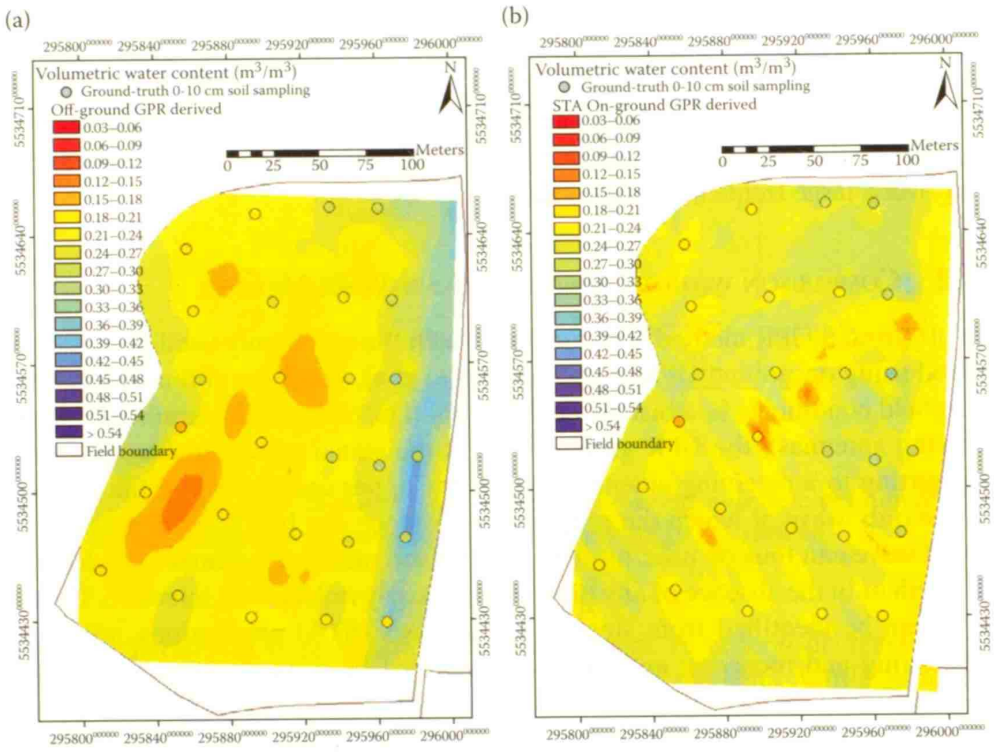

FIGURE 2.5 Comparison between the off-ground GPR full-waveform inversion (a) and the on-ground GPR STA approach (b) for soil moisture mapping at the field scale.

2.4.3 Comparison with Ground-Based Radiometry

Ground-based sensors are particularly necessary for improving and validating large-scale remote sensing data products. Passive microwave sensors were mainly developed for spaceborne remote sensing of soil moisture, but ground-based radiometers were also applied at the field scale. In that respect, we compared the off-ground GPR system with an L-band radiometer to map surface soil moisture at the field scale (Jonard et al. 2011). The experiment was conducted on a bare agricultural field at the Selhausen test site of the Forschungszentrum Jülich GmbH (Germany) on July 14, 2009. GPR and L-band radiometer data were collected on a 72 × 16 m^2 experimental plot consisting of eight transects with 18 measurement points each. In addition, TDR measurements were performed within the footprints of the GPR and the radiometer as ground-truth information. The off-ground GPR and the L-band radiometer JÜLBARA were mounted on the back of a truck (Figure 2.6). The Dicke-type radiometer JÜLBARA was equipped with a dual-mode conical horn antenna (aperture diameter = 68 cm, length = 61 cm). The radiometer antenna aperture was situated about 2 m above the soil surface and directed with an observation angle of 53° relative to the vertical direction. The GPR antenna aperture was about 1.2 m above the ground with normal incidence. The brightness temperature (T_B) measured with the radiometer was used to derive the soil surface dielectric permittivity. T_B was measured at horizontal and vertical polarizations in the frequency range of

FIGURE 2.6 GPR and L-band radiometer mounted on a truck to measure surface soil relative dielectric permittivity. (Adapted from Jonard, F. et al., *IEEE Transactions on Geosciences and Remote Sensing*, 49(8), 2863–2875, 2011.)

1.400–1.427 GHz. For GPR, the dielectric permittivity was retrieved using inversion of the radar data in the time domain, focusing on the surface reflection.

The estimated surface soil moisture from GPR, radiometer (considering the average between the horizontal and vertical polarizations), and TDR measurements are displayed in Figure 2.7. Although the overall soil moisture patterns were reasonably well reproduced by the three techniques, significant differences in the absolute

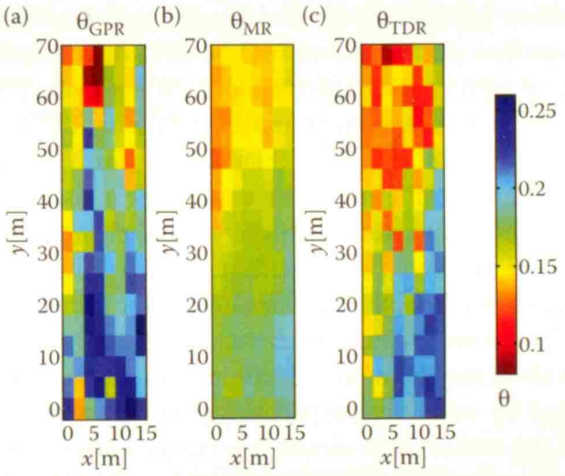

FIGURE 2.7 Volumetric soil moisture maps obtained using (a) off-ground GPR, (b) radiometer (averaged over both polarizations), and (c) TDR measurements at the Selhausen test site. (Adapted from Jonard, F. et al., *IEEE Transactions on Geosciences and Remote Sensing*, 49(8), 2863–2875, 2011.)

moisture values were observed. These discrepancies can be attributed to different sensing depths and footprint areas and different sensitivities to soil surface roughness. For GPR, the effect of roughness was excluded by operating at low frequencies (0.2–0.8 GHz) that were not sensitive to the field surface roughness according to Rayleigh's criterion. The RMSE between volumetric soil moisture measured by GPR and TDR was 0.038 m^3/m^3. For the radiometer, the RMSE decreased from 0.062 m^3/m^3 (horizontal polarization) and 0.054 m^3/m^3 (vertical polarization) to 0.020 m^3/m^3 (both polarizations) after accounting for roughness using an empirical model that required calibration with reference TDR measurements (see Jonard et al. 2011 for details). Relatively accurate soil moisture retrievals were possible with the off-ground GPR and L-band radiometer, although accounting for surface roughness was essential for the L-band radiometer. Future improvements may focus on the potential radiometer and GPR synergies for improving soil moisture estimates, to be applied, for instance, in the upcoming NASA's Soil Moisture Active Passive mission.

2.4.4 Soil Moisture Profile Characterization

For most hydrologic and agricultural applications, it is more relevant to characterize the root-zone soil moisture (0–30 cm) rather than shallow surface soil moisture (0–10 cm; Vereecken et al. 2008). In addition, decoupling of surface and subsurface soil moisture may occur under various specific conditions such as the case when considering a wet soil subject to fast evaporation or the propagation of a wetting front in a dry soil, especially in coarse materials (Capehart and Carlson 1997). In that respect, the relatively low frequency of the GPR allows a larger penetration depth than remote sensing instruments. Moreover, owing to the large frequency bandwidth of the ultrawideband GPR system that we used, information over different depths can be retrieved from the GPR data.

GPR data inversion accounting for two-layered and continuously varying soil moisture profile was thus performed with GPR field data acquired over a layered soil in an agricultural field in Walhain, Belgium (Minet et al. 2011) using the same off-ground GPR approach as presented above. Following dry conditions, the shallow surface soil was crusted and drier than the subsurface soil. Figure 2.8 presents the two-layered and profile model inversion soil moisture maps. Surface and subsurface soil moisture maps from two-layered and profile inversions showed, in general, a coherent soil moisture profile with respect to terrain observations, that is, soil moisture increases with depth. The subsurface (or second layer) soil moisture was characterized by a lower spatial coherence, with a larger nugget effect, denoting that retrieved values may be more uncertain than the surface (or first layer) soil moisture, as outlined by numerical experiments (not shown). The first-layer thicknesses retrieved in the two-layered model inversions were in good agreement with the depths of inflexion points of soil moisture profiles in the profile model inversions and were on average, about 4 cm. Except for some particular difference, the surface soil moisture retrieved by the two-layered or profile model inversions appeared very similar, whereas the subsurface (or second layer) soil moisture differed between the two model inversions. When assuming a homogeneous soil medium, the retrieved

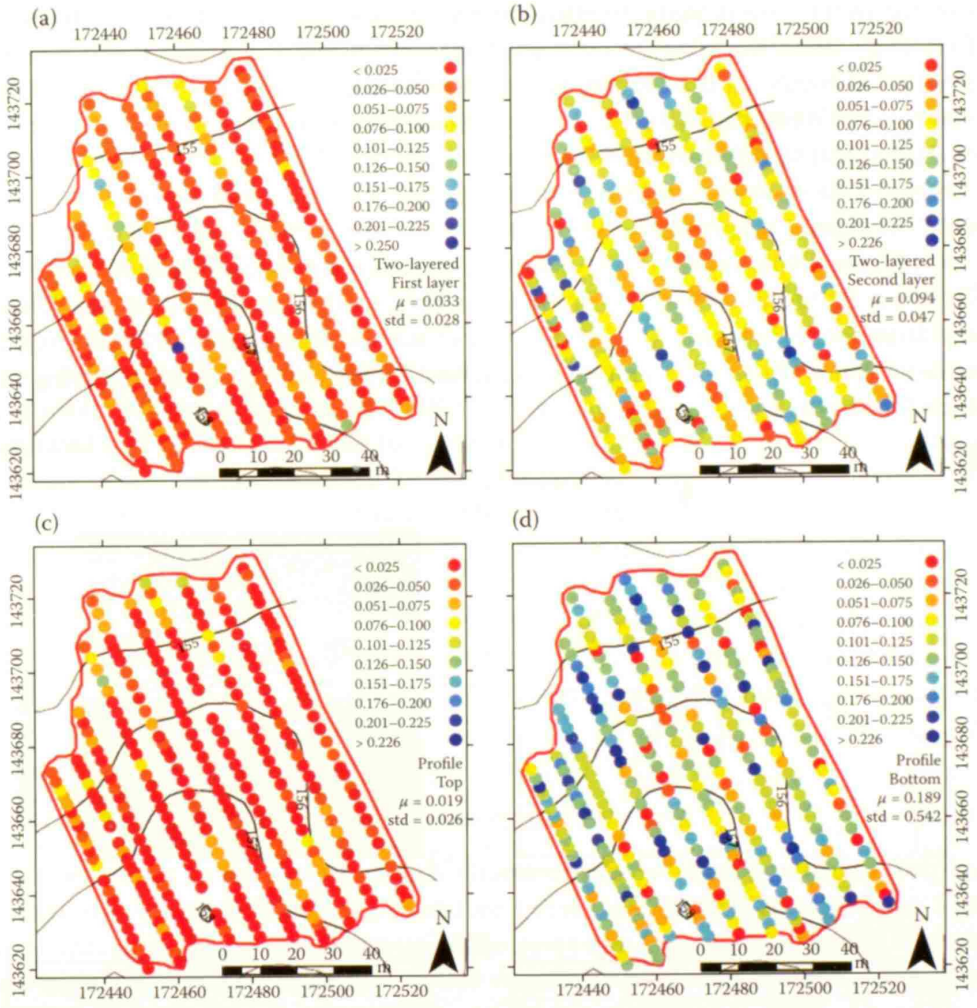

FIGURE 2.8 Soil moisture maps from two-layered model inversions for the first layer (a) and the second layer (b) and from the profile model inversions for the top (c) and the bottom (d) of the profile. (Adapted from Minet, J. et al., *Geoderma*, 161, 225–237, 2011.)

soil moisture was, in general, in the intermediate range between surface and subsurface soil moisture (not shown). The agreement between the different model inversions indicated the well posedness of the GPR inversion for determining multilayered soil properties.

2.4.5 Time-Lapse GPR Monitoring

In field conditions, Jadoon et al. (2010) performed repeated GPR measurements for 20 days with a time step of 15 min in order to monitor the dynamics of the near-surface soil moisture content. The off-ground GPR antenna was installed 1 m above the ground, and the surface of the soil was exposed to natural processes, that is, precipitation and evaporation. The permittivity of the soil was estimated by GPR data

inversion in the time domain, focusing on the surface reflection. Topp's relationship (Topp et al. 1980; Equation 2.5) was used to infer soil moisture from inversely estimated permittivity. At the same field site, Topp's relationship was known to provide good results (Weihermüller et al. 2007), with an RMSE of 0.021 m^3/m^3 between the volumetric soil sample and TDR estimates.

Figure 2.9a shows the hourly observation of precipitation and potential evaporation. Three major precipitation events occurred during the time-lapse GPR measurements. Figure 2.9b shows the GPR data in the time domain. The effect of precipitation events can be visually observed in the radar data, as they resulted in strong reflections from the soil surface. The permittivity of the soil increased with moisture, and the radar signal shows high amplitude of reflection from the soil surface during the time of precipitation.

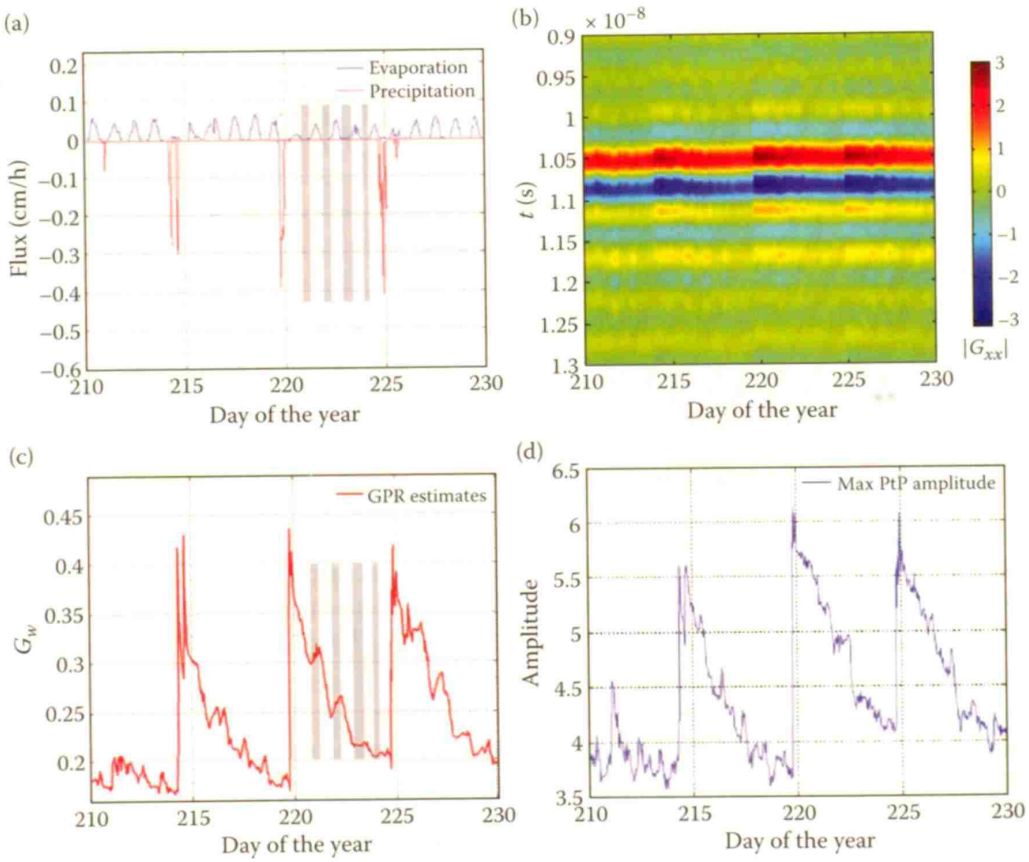

FIGURE 2.9 (a) Precipitation and evaporation flux values (negative for downward flux) as a function of days of the year recorded over a 20-day period (meteorological station at Selhausen, Germany), (b) measured Green's function represented in the time domain with a measurement time step of 15 min, (c) water content inferred from a GPR signal inversion, and (d) maximum PtP reflection recorded in a time-domain GPR signal. In (a) and (c), the gray patches correspond to the time when there was almost no evaporation. (Adapted from Jadoon, K. Z. et al., *Near Surface Geophysics*, 8(6), 483–491, 2010.)

Figure 2.9c shows the soil moisture inferred from time-lapse GPR measurements. The top few centimeters of the soil were sensitive to evaporation and dried more rapidly. This effect can be observed by the faster decrease in the GPR-derived soil moisture. During the night, a slight increase in the surface soil moisture occurred, most likely because of the dew, which can be observed in the GPR-estimated soil moisture. For instance, in Figure 2.9a, four gray patches represent the periods when there was almost no evaporation. These periods are highlighted in Figure 2.9c, showing the corresponding slight increase in the GPR-derived water content. Three undisturbed cylindrical samples of 100 cm^3 were extracted near the time-lapse GPR setup. The mean saturated soil moisture estimated from the three soil samples was 0.412 m^3/m^3. At the time of the precipitation events, the mean of the three maximum soil moisture estimated by GPR was 0.426 m^3/m^3, which is very close to the saturated soil moisture inferred from the soil samples. The slight difference in the saturated soil moisture obtained by the two methods may be due to the different characterization scales, soil spatial variability, and the petrophysical model relating dielectric permittivity to water content, or a combination of these three major factors. Figure 2.9d depicts the maximum peak-to-peak (PtP) amplitude of the signal recorded between 10.5 and 11.0 ns in Figure 2.9b. The trend of the PtP amplitude corresponded well to the evaporation and precipitation events. The maximum PtP amplitude can be observed during precipitation events, and the decreasing trend shows the effect of evaporation.

2.4.6 Temporal Stability of Soil Moisture Patterns

Soil moisture is an ephemeral variable characterized by a high spatial and temporal variability. When installing soil moisture point measurement devices (e.g., TDR and capacitance probes), representative locations of a field or catchment in terms of soil moisture would be preferred. In that respect, several authors have investigated the temporal stability of soil moisture pattern (e.g., Guber et al. 2008). Using time-lapse GPR measurements, we characterized the spatiotemporal soil moisture distribution in a 2.5-ha agricultural field in Vieusart, Belgium, using five high-resolution acquisitions of GPR data in March and April 2010 (Minet et al. in preparation; Figure 2.10).

The first three dates were characterized by dry conditions, whereas rainfalls were observed the day before the fourth date. In Figure 2.10, zones where interpolated soil moisture values are equal to the field average (± 0.01 m^3/m^3) are outlined by black hatched areas. These zones intersect between the five dates (orange areas), indicating time-stable locations for the field average soil moisture. There was a remarkable temporal stability of soil moisture patterns for the first three and the two last dates, respectively. However, due to moderate rainfalls (24.8 mm), the soil moisture pattern largely changed between the third and fourth dates. In particular, the zones indicating the spatial-average soil moisture shrank from dry to wet conditions as the standard deviation of soil moisture increased. Finally, the time-stable zones indicating the field average appeared to be located in mid-slopes areas, as already noticed by Jacobs et al. (2004). Nevertheless, field acquisitions in other seasons are needed to

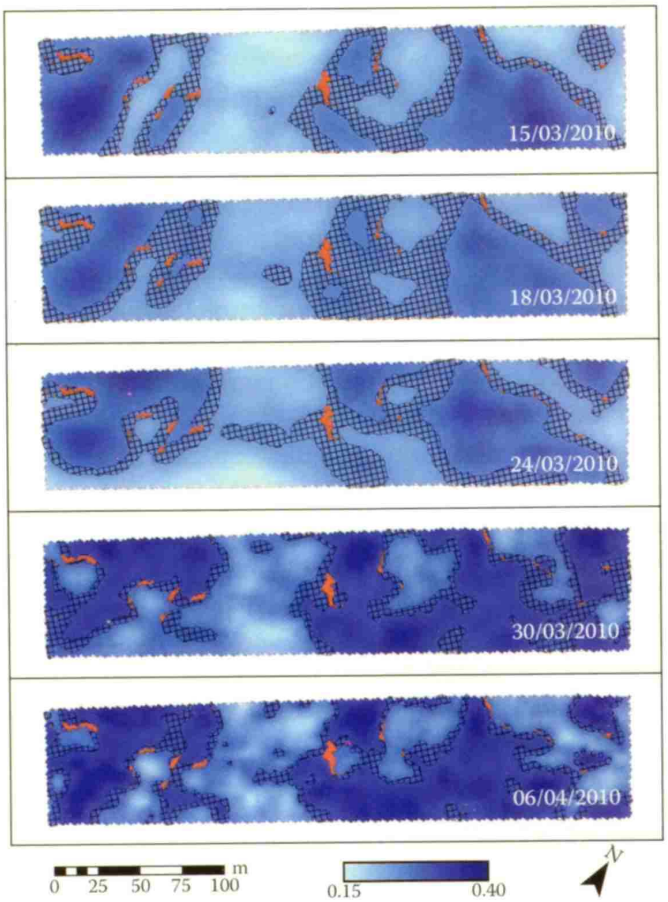

FIGURE 2.10 Soil moisture maps in a 2.5-ha field in Vieusart, Belgium, for five dates in March and April 2010. Temporal stability of field average soil moisture (± 0.01 m^3/m^3) is outlined by hatched areas. (Adapted from Minet, J. et al., Spatiotemporal pattern of soil moisture measured by a proximal GPR in an agricultural field, in preparation.)

fully investigate soil moisture patterns and to relate them to soil and/or topographic attributes.

2.5 CONCLUSIONS

In this chapter, we emphasized the high capabilities of GPR for soil moisture characterization at the field scale in order to bridge the scale gap in soil moisture sensing between large-scale remote sensing platforms and small-scale invasive sensors. We presented an advanced off-ground GPR method for quantitatively measuring soil moisture based on the VNA technology and an accurate 3-D modeling of GPR wave propagation in the antenna–soil system. It is worth noting that this GPR approach also applies to common time-domain GPR systems. This proximal sensing GPR method proved to be particularly appropriate for soil moisture mapping at

a high spatial resolution at the field scale due to its rapidity and to the air-launched configuration of the antenna. The soil moisture measurements were found to be highly accurate and precise when comparing with the ground-truth measurements and repeating the acquisition. The relatively large footprint of the GPR antenna allows for integrating the soil moisture measurement at a larger support scale than invasive sensors. When compared to commonly used ground-wave analysis based on on-ground GPR, the observed differences were mainly attributed to the different depths of characterization. The off-ground GPR system resulted in similar soil moisture maps compared to ground-based radiometry, whereas the latter technique required ground-truth measurements of soil moisture for calibration with respect to the surface roughness characterization. The large frequency bandwidth at which the GPR operates allowed for maximizing the information retrieval capabilities and, especially, to characterize a two-layered or continuously varying moisture profile. The off-ground GPR was also used for time-lapse measurements of soil moisture that were interpreted according to meteorological conditions. Finally, time-lapse measurements over a field allowed for revealing the temporal stability of soil moisture patterns. This tool is promising for studying the spatiotemporal variability of soil moisture at the field scale, validation of remote sensing of soil moisture products, improvement of hydrologic modeling through data assimilation, and precision agriculture and irrigation applications. In particular, high-spatial-resolution GPR acquisitions may be combined with high-temporal-resolution grounded sensor networks for an unprecedented spatiotemporal characterization of soil moisture patterns.

ACKNOWLEDGMENTS

This work was supported by the Université Catholique de Louvain (Belgium), Forchungszentrum Jülich GmbH (Germany), Delft University of Technology (The Netherlands), the Belgian Science Policy Office in the frame of the Stereo II Programme—Project SR/00/100 (HYDRASENS), the DIGISOIL Project financed by the European Commission under the 7th Framework Programme for Research and Technological Development, Area "Environment," Activity 6.3 "Environmental Technologies," the German Research Foundation (DFG) in the frame of Transregional Collaborative Research Centre 32, and the Fonds de la Recherche Scientifique (FNRS; Belgium).

REFERENCES

Alumbaugh, D., Chang, P., Paprocki, L., Brainard, J., Glass, R. J., and Rautman, C. A. (2002). Estimating moisture contents in the vadose zone using cross-borehole ground penetrating radar: A study of accuracy and repeatability. *Water Resources Research*, 38, 1309.

Benedetto, A. (2010). Water content evaluation in unsaturated soil using GPR signal analysis in the frequency domain. *Journal of Applied Geophysics*, 71, 26–35.

Binley, A., Cassiani, G., Middleton, R., and Winship, P. (2002). Vadose zone flow model parameterisation using cross-borehole radar and resistivity imaging. *Journal of Hydrology*, 267, 147–159.

Binley, A., Winship, P., Middleton, R., Pokar, M., and West, J. (2001). High-resolution characterization of vadose zone dynamics using cross-borehole radar. *Water Resources Research*, 37, 2639–2652.

Birchak, J. R., Gardner, C. G., Hipp, J. E., and Victor, J. M. (1974). High dielectric-constant microwave probes for sensing soil-moisture. *Proceedings of the IEEE*, 62(1), 93–98.

Bogena, H., Herbst, M., Huisman, J., Rosenbaum, U., Weuthen, A., and Vereecken, H. (2010). Potential of wireless sensor networks for measuring soil water content variability. *Vadose Zone Journal*, 9, 1002–1013.

Bogena, H. R., Huisman, J. A., Oberdoerster, C., and Vereecken, H. (2007). Evaluation of a low-cost soil water content sensor for wireless network applications. *Journal of Hydrology*, 344(1–2), 32–42.

Campbell, G. S., Calissendorff, C., and Williams, J. H. (1991). Probe for measuring soil specific heat using a heat-pulse method. *Soil Science Society of America Journal*, 55(1), 291–293.

Capehart, W. J. and Carlson, T. N. (1997). Decoupling of surface and near-surface soil water content: A remote sensing perspective. *Water Resources Research*, 33(6), 1383–1395.

Cassiani, G. and Binley, A. (2005). Modeling unsaturated flow in a layered formation under quasi-steady-state conditions using geophysical data constraints. *Advances in Water Resources*, 28, 467–477.

Cassidy, N. J. (2007). Evaluating LNAPL contamination using GPR signal attenuation analysis and dielectric property measurements: Practical implications for hydrological studies. *Journal of Contaminant Hydrology*, 94, 49–75.

Ceballos, A., Scipal, K., Wagner, W., and Martinez-Fernandez, J. (2005). Validation of ERS scatterometer-derived soil moisture data in the central part of the Duero Basin, Spain. *Hydrological Processes*, 19(8), 1549–1566.

Chanzy, A., Tarussov, A., Judge, A., and Bonn, F. (1996). Soil water content determination using digital ground penetrating radar. *Soil Science Society of America Journal*, 60, 1318–1326.

Davis, J. L. and Annan, A. P. (1989). Ground penetrating radar for high-resolution mapping of soil and rock stratigraphy. *Geophysical Prospecting*, 37, 531–551.

Dirksen, C. and Dasberg, S. (1993). Improved calibration of time-domain reflectometry soil-water content measurements. *Soil Science Society of America Journal*, 57(3), 660–667.

Dobson, M. C., Ulaby, F. T., Hallikainen, M. T., and Elrayes, M. A. (1985). Microwave dielectric behavior of wet soil—Part II: Dielectric mixing models. *IEEE Transactions on Geoscience and Remote Sensing*, 23(1), 35–46.

Doolittle, J. A., Jenkinson, B., Hopkins, D., Ulmer, M., and Tuttle, W. (2006). Hydropedological investigations with ground-penetrating radar (GPR): Estimating water-table depths and local ground-water flow pattern in areas of coarse-textured soils. *Geoderma*, 131(3–4), 317–329.

Drungil, C. E. C., Abt, K., and Gish, T. J. (1989). Soil-moisture determination in gravelly soils with time-domain reflectometry. *Transactions of the ASAE*, 32(1), 177–180.

Fernandez-Galvez, J. (2008). Errors in soil moisture content estimates induced by uncertainties in the effective soil dielectric constant. *International Journal of Remote Sensing*, 29(11), 3317–3323.

Galagedara, L. W., Parkin, G. W., and Redman, J. D. (2003). An analysis of the GPR direct ground wave method for soil water content measurement. *Hydrological Processes*, 17, 3615–3628.

Galagedara, L. W., Parkin, G. W., Redman, J. D., von Bertoldi, P., and Endres, A. L. (2005a). Field studies of the GPR ground wave method for estimating soil water content during irrigation and drainage. *Journal of Hydrology*, 301, 182–197.

Galagedara, L. W., Redman, J. D., Parkin, G. W., Annan, A. P., and Endres, A. L. (2005b). Numerical modeling of GPR to determine the direct ground wave sampling depth. *Vadose Zone Journal*, 4, 1096–1106.

Garrido, F., Ghodrati, M., and Chendorain, M. (1999). Small-scale measurement of soil water content using a fiber optic sensor. *Soil Science Society of America Journal*, 63(6), 1505–1512.

Gorriti, A. G. (2004). *Electric Characterization of Sands with Heterogeneous Saturation Distribution*. PhD thesis, Delft University of Technology, Delft, The Netherlands, 202 pp.

Grandjean, G., Paillou, P., Baghdadi, N., Heggy, E., August, T., and Lasne, Y. (2006). Surface and subsurface structural mapping using low-frequency radar: A synthesis of the Mauritanian and Egyptian experiments. *Journal of African Earth Sciences*, 44, 220–228.

Grote, K., Anger, C., Kelly, B., Hubbard, S., and Rubin, Y. (2010). Characterization of soil water content variability and soil texture using GPR groundwave techniques. *Journal of Environmental and Engineering Geophysics*, 15(3, Sp. Iss. SI), 93–110.

Grote, K., Hubbard, S. S., and Rubin, Y. (2003). Field-scale estimation of volumetric water content using GPR groundwave techniques. *Water Resources Research*, 39(11), 1321.

Guber, A. K., Gish, T. J., Pachepsky, Y. A., Van Genuchten, M. T., Daughtry, C. S. T., Nicholson, T. J., and Cady, R. E. (2008). Temporal stability in soil water content patterns across agricultural fields. *Catena*, 73, 125–133.

al Hagrey, S. A. and Müller, C. (2000). GPR study of pore water content and salinity in sand. *Geophysical Prospecting*, 48, 63–85.

Hallikainen, M. T., Ulaby, F. T., Dobson, M. C., Elrayes, M. A., and Wu, L. K. (1985). Microwave dielectric behavior of wet soil—Part I: Empirical models and experimental observations. *IEEE Transactions on Geoscience and Remote Sensing*, 23(1), 25–34.

Huisman, J. A., Hubbard, S. S., Redman, J. D., and Annan, A. P. (2003). Measuring soil water content with ground penetrating radar: A review. *Vadose Zone Journal*, 2, 476–491.

Huisman, J. A., Snepvangers, J. J. J. C., Bouten, W., and Heuvelink, G. B. M. (2002). Mapping spatial variation in surface soil water content: Comparison of ground-penetrating radar and time-domain reflectometry. *Journal of Hydrology*, 269, 194–207.

Hupet, F. and Vanclooster, M. (2002). Intraseasonal dynamics of soil moisture variability within a small agricultural maize cropped field. *Journal of Hydrology*, 261(1–4), 86–101.

Huyer, W. and Neumaier, A. (1999). Global optimization by multilevel coordinate search. *Journal of Global Optimization*, 14(4), 331–355.

Jacob, R. W. and Hermance, J. F. (2004). Assessing the precision of GPR velocity and vertical two-way travel time estimates. *Journal of Environmental and Engineering Geophysics*, 9, 143–153.

Jacobs, J. M., Mohanty, B. P., Hsu, E. C., and Miller, D. (2004). SMEX02: Field scale variability, time stability and similarity of soil moisture. *Remote Sensing of Environment*, 92, 436–446.

Jadoon, K. Z., Lambot, S., Scharnagl, B., van der Kruk, J., Slob, E., and Vereecken, H. (2010). Quantifying field-scale surface soil water content from proximal GPR signal inversion in the time domain. *Near Surface Geophysics*, 8(6), 483–491, doi:10.3997/1873-0604.2010036.

Jadoon, K., Lambot, S., Slob, E., and Vereecken, H. (2008). Uniqueness and stability analysis of hydrogeophysical inversion for time-lapse proximal ground penetrating radar. *Water Resources Research*, 44, W0942.

Jadoon, K. Z., Slob, E., Vereecken, H., and Lambot, S. (2011). Analysis of antenna transfer functions and phase center position for modeling off-ground GPR. *IEEE Transactions on Geosciences and Remote Sensing*, 48(5), 1649–1662, doi:10.1109/TGRS.2010.2089691.

Jonard, F., Weihermüller, L., Jadoon, K. Z., Schwank, M., Vereecken, H., and Lambot, S. (2011). Mapping field scale soil moisture with L-band radiometer and ground-penetrating radar GPR over bare soil. *IEEE Transactions on Geosciences and Remote Sensing*, 49(8), 2863–2875.

Jonard, F., Weihermüller, L., Vereecken, H., and Lambot, S. (in press). Accounting for soil surface roughness in the inversion of ultra-wideband off-ground GPR signal for soil moisture retrieval. *Geophysics*.

Kowalsky, M. B., Finsterle, S., Peterson, J., Hubbard, S., Rubin, Y., Majer, E., Ward, A., and Gee, G. (2005). Estimation of field-scale soil hydraulic and dielectric parameters through joint inversion of GPR and hydrological data. *Water Resources Research*, 41, W11425.

Lagarias, J. C., Reeds, J. A., Wright, M. H., and Wright, P. E. (1998). Convergence properties of the Nelder–Mead Simplex method in low dimensions. *Siam Journal on Optimization*, 9(1), 112–147.

Lambot, S., Rhebergen, J., van den Bosch, I., Slob, E. C., and Vanclooster, M. (2004b). Measuring the soil water content profile of a sandy soil with an off-ground monostatic ground penetrating radar. *Vadose Zone Journal*, 3(4), 1063–1071.

Lambot, S., Slob, E. C., Chavarro, D., Lubczynski, M., and Vereecken, H. (2008). Measuring soil surface water content in irrigated areas of southern Tunisia using full-waveform inversion of proximal GPR data. *Near Surface Geophysics*, 6, 403–410.

Lambot, S., Slob, E. C., Rhebergen, J., Lopera, O., Jadoon, K. Z., and Vereecken, H. (2009). Remote estimation of the hydraulic properties of a sand using full-waveform integrated hydrogeophysical inversion of time-lapse, off-ground GPR data. *Vadose Zone Journal*, 8, 743–754.

Lambot, S., Slob, E. C., van den Bosch, I., Stockbroeckx, B., and Vanclooster, M. (2004a). Modeling of ground-penetrating radar for accurate characterization of subsurface electric properties. *IEEE Transactions on Geoscience and Remote Sensing*, 42, 2555–2568.

Lambot, S., Slob, E. C., and Vereecken, H. (2007). Fast evaluation of zero-offset Green's function for layered media with application to ground-penetrating radar. *Geophysical Research Letters*, 34, L21405, doi:10.1029/2007GL031459.

Lambot, S., Weihermüller, L., Huisman, J. A., Vereecken, H., Vanclooster, M., and Slob, E. C. (2006). Analysis of air-launched ground-penetrating radar techniques to measure the soil surface water content. *Water Resources Research*, 42, W11403.

Lehmann, F. and Green, A. G. (1999). Semiautomated georadar data acquisition in three dimensions. *Geophysics*, 64, 719–731.

Looms, M. C., Jensen, K. H., Binley, A., and Nielsen, L. (2008). Monitoring unsaturated flow and transport using cross-borehole geophysical methods. *Vadose Zone Journal*, 7(1), 227–237.

Lunt, I. A., Hubbard, S. S., and Rubin, Y. (2005). Soil moisture content estimation using ground-penetrating radar reflection data. *Journal of Hydrology*, 307(1–4), 254–269.

Martinez, G., Vanderlinden, K., Giráldez, J. V., Espejo, A. J., and Muriel, J. L. (2010). Field-scale soil moisture pattern mapping using electromagnetic induction. *Vadose Zone Journal*, 9, 871–881.

Michot, D., Benderitter, Y., Dorigny, A., Nicoullaud, B., King, D., and Tabbagh, A. (2003). Spatial and temporal monitoring of soil water content with an irrigated corn crop cover using surface electrical resistivity tomography. *Water Resources Research*, 39(5), 1138, doi:10.1029/2002WR001581.

Minet, J., Lambot, S., Slob, E., and Vanclooster, M. (2010). Soil surface water content estimation by full-waveform GPR signal inversion in the presence of thin layers. *IEEE Transactions on Geoscience and Remote Sensing*, 48, 1138–1150.

Minet, J., Vanclooster, M., and Lambot, S. (in preparation). Spatiotemporal pattern of soil moisture measured by a proximal GPR in an agricultural field.

Minet, J., Wahyudi, A., Bogaert, P., Vanclooster, M., and Lambot, S. (2011). Mapping shallow soil moisture profiles at the field scale using full-waveform inversion of ground penetrating radar data. *Geoderma*, 161, 225–237, doi:10.1016/j.geoderma.2010.12.023.

Oden, C. P., Olhoeft, G. R., Wright, D. L., and Powers, M. H. (2008). Measuring the electrical properties of soil using a calibrated ground-coupled GPR system. *Vadose Zone Journal*, 7, 171–183.

Ponizovsky, A. A., Chudinova, S. M., and Pachepsky, Y. A. (1999). Performance of TDR calibration models as affected by soil texture. *Journal of Hydrology*, 218(1–2), 35–43.

Robinson, D. A., Binley, A., Crook, N., Day-Lewis, F. D., Ferre, T. P. A., Grauch, V. J. S., Knight, R., Knoll, M., Lakshmi, V., Miller, R., Nyquist, J., Pellerin, L., Singha, K., and Slater, L. (2008a). Advancing process-based watershed hydrological research using near-surface geophysics: A vision for, and review of, electrical and magnetic geophysical methods. *Hydrological Processes*, 22(18), 3604–3635.

Robinson, D. A., Campbell, C. S., Hopmans, J. W., Hornbuckle, B. K., Jones, S. B., Knight, R., Ogden, F., Selker, J., and Wendroth, O. (2008b). Soil moisture measurement for ecological and hydrological watershed-scale observatories: A review. *Vadose Zone Journal*, 7(1), 358–389.

Robinson, D. A., Jones, S. B., Wraith, J. M., Or, D., and Friedman, S. P. (2003). A review of advances in dielectric and electrical conductivity measurement in soils using time-domain reflectometry. *Vadose Zone Journal*, 2, 444–475.

Roth, C. H., Malicki, M. A., and Plagge, R. (1992). Empirical evaluation of the relationship between soil dielectric-constant and volumetric water content as the basis for calibrating soil-moisture measurements by TDR. *Journal of Soil Science*, 43(1), 1–13.

Roth, K., Schulin, R., Fluhler, H., and Attinger, W. (1990). Calibration of time-domain reflectometry for water-content measurement using a composite dielectric approach. *Water Resources Research*, 26(10), 2267–2273.

Saintenoy, A., Schneider, S., and Tucholka, P. (2008). Evaluating ground-penetrating radar use for water infiltration monitoring. *Vadose Zone Journal*, 7, 208–214.

Serbin, G. and Or, D. (2003). Near-surface water content measurements using horn antenna radar: Methodology and overview. *Vadose Zone Journal*, 2, 500–510.

Serbin, G. and Or, D. (2005). Ground-penetrating radar measurement of crop and surface water content dynamics. *Remote Sensing of Environment*, 96, 119–134.

Shutko, A. M. and Reutov, E. M. (1982). Mixture formulas applied in estimation of dielectric and radiative characteristics of soils and grounds at microwave-frequencies. *IEEE Transactions on Geoscience and Remote Sensing*, 20(1), 29–32.

Slob, E. C. and Fokkema, J. (2002). Coupling effects of two electric dipoles on an interface. *Radio Science*, 37(5), 1073, doi:10.1029/2001RS2529.

Slob, E. C., Sato, M., and Olhoeft, G. (2010). Surface and borehole ground-penetrating radar developments. *Geophysics*, 75(5), A103–A120.

Steelman, C. M. and Endres, A. L. (2011). Comparison of petrophysical relationships for soil moisture estimation using GPR ground waves. *Vadose Zone Journal*, 10(1), 270–285.

Todoroff, P. and Langellier, P. (1998). Comparison of empirical and partly deterministic methods of time domain reflectometry calibration, based on a study of two tropical soils. *Soil and Tillage Research*, 45(3–4), 325–340.

Topp, G. C., Davis, J. L., and Annan, A. P. (1980). Electromagnetic determination of soil water content: Measurements in coaxial transmission lines. *Water Resources Research*, 16, 574–582.

van der Kruk, J. (2006). Properties of surface waveguides derived from inversion of fundamental and higher mode dispersive GPR data. *IEEE Transactions on Geoscience and Remote Sensing*, 44(10), 2908–2915.

van der Kruk, J., Arcone, S. A., and Liu, L. (2007). Fundamental and higher mode inversion of dispersed GPR waves propagating in an ice layer. *IEEE Transactions on Geoscience and Remote Sensing*, 45(8), 2483–2491.

van Overmeeren, R. A., Sariowan, S. V., and Gehrels, J. C. (1997). Ground penetrating radar for determining volumetric soil water content: Results of comparative measurements at two test sites. *Journal of Hydrology*, 197, 316–338.

Vereecken, H., Huisman, J. A., Bogena, H., Vanderborght, J., Vrugt, J. A., and Hopmans, J. W. (2008). On the value of soil moisture measurements in vadose zone hydrology: A review. *Water Resources Research*, 44, W00D06.

Verhoest, N. E. C., Lievens, H., Wagner, W., Alvarez-Mozos, J., Moran, M. S., and Mattia, F. (2008). On the soil roughness parameterization problem in soil moisture retrieval of bare surfaces from synthetic aperture radar. *Sensors*, 8(7), 4213–4248.

Wagner, W., Blöschl, G., Pampaloni, P., Calvet, J. C., Bizzarri, B., Wigneron, J. P., and Kerr, Y. (2007). Operational readiness of microwave remote sensing of soil moisture for hydrologic applications. *Nordic Hydrology*, 38(1), 1–20.

Weihermüller, L., Huisman, J. A., Lambot, S., Herbst, M., and Vereecken, H. (2007). Mapping the spatial variation of soil water content at the field scale with different ground penetrating radar techniques. *Journal of Hydrology*, 340, 205–216.

Weiler, K. W., Steenhuis, T. S., Boll, J., and Kung, K. J. S. (1998). Comparison of ground penetrating radar and time domain reflectometry as soil water sensors. *Soil Science Society of America Journal*, 62, 1237–1239.

Wigneron, J. P., Calvet, J. C., Pellarin, T., Van de Griend, A. A., Berger, M., and Ferrazzoli, P. (2003). Retrieving near-surface soil moisture from microwave radiometric observations: current status and future plans. *Remote Sensing of Environment*, 85(4), 489–506.

Windsor, C., Capineri, L., Falorni, P., Matucci, S., and Borgioli, G. (2005). The estimation of buried pipe diameters using ground penetrating radar. *Insight*, 47, 394–399.